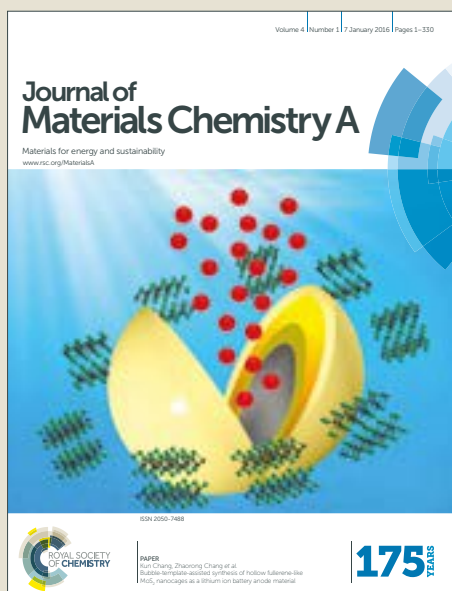


Journal of Materials Chemistry A

Accepted Manuscript



This article can be cited before page numbers have been issued, to do this please use: M. Tsai, C. Wang, C. Chang, C. Hsu, Y. Hsiao, C. Liu, C. Wang, S. Lin and C. Lin, *J. Mater. Chem. A*, 2017, DOI: 10.1039/C7TA09322E.



This is an Accepted Manuscript, which has been through the Royal Society of Chemistry peer review process and has been accepted for publication.

Accepted Manuscripts are published online shortly after acceptance, before technical editing, formatting and proof reading. Using this free service, authors can make their results available to the community, in citable form, before we publish the edited article. We will replace this Accepted Manuscript with the edited and formatted Advance Article as soon as it is available.

You can find more information about Accepted Manuscripts in the [author guidelines](#).

Please note that technical editing may introduce minor changes to the text and/or graphics, which may alter content. The journal's standard [Terms & Conditions](#) and the ethical guidelines, outlined in our [author and reviewer resource centre](#), still apply. In no event shall the Royal Society of Chemistry be held responsible for any errors or omissions in this Accepted Manuscript or any consequences arising from the use of any information it contains.



Journal Name

ARTICLE

A Large, Ultra Black, Efficient and Cost-effective Dye-sensitized Solar Module Approaching 12% Overall Efficiency under 1000 Lux Indoor Light

Received 00th January 20xx,
Accepted 00th January 20xx

DOI: 10.1039/x0xx00000x

www.rsc.org/

Ming-Chi Tsai,^a Chin-Li Wang,^{a,b} Chiung-Wen Chang,^a Cheng-Wei Hsu,^b Yu-Hsin Hsiao,^a Chia-Lin Liu,^a Chen-Chi Wang,^a Shr-Yau Lin,^a Ching-Yao Lin*^a

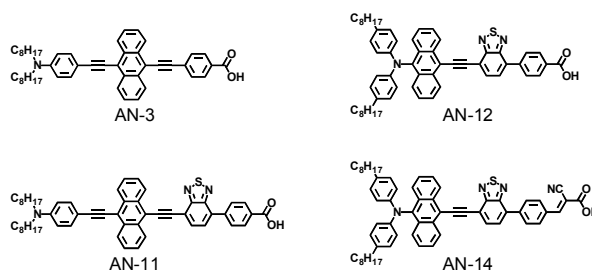
Three novel anthracene-based organic dyes, denoted as AN-11, AN-12 and AN-14, were synthesized for outdoor and indoor dye-sensitized solar cell studies. Laboratory-fabricated small cells, as well as rigid and flexible modules were prepared and analyzed for their photovoltaic performance under simulated outdoor and indoor conditions. Owing to the panchromatic absorption of visible light, the AN-11 module gives rise to a very black color and superior photovoltaic performance. Significantly, the AN-11 rigid module with a large active area of 26.80 cm² outperforms the Z907 counterpart under indoor conditions, reaching an overall efficiency of 11.94% under 1000 lux of T5 fluorescent light. In addition, the AN-11 module exhibits good stability during the weather stress tests. Finally, the AN-11 dye is cost-effective and our studies show that photovoltaic performance of the solar cells are not affected upon lowering the synthetic cost and increasing the synthetic scale.

Introduction

Dye-sensitized solar cell (DSSC) has been widely studied in recent decades owing to the low production costs, simple manufacturing processes and vivid colours of the dyes.¹⁻⁴ Numerous dyes have been reported to achieve high photovoltaic performance in DSSC under 100 mW/cm² simulated AM1.5G sunlight (or one-sun), including ruthenium complexes,⁵⁻⁹ zinc porphyrins¹⁰⁻¹⁶ and metal-free organic dyes.¹⁷⁻¹⁹ Among these dyes, organic dyes have been widely studied owing to the advantages of possibly higher extinction coefficients (than those of the ruthenium complexes), versatile molecular design and low synthetic costs. For the purposes of efficient charge transfer and electron injection, chemical structures of the organic dyes are often designed in a donor- π -acceptor (or D- π -A) fashion. In addition to the obvious roles of the donors and acceptors, the π -spacers also play an important part of light harvesting.^{20,21} Many π -spacers have been reported to be useful, including EDOT (C217),²² thiophene (JK-46),²³ fluorene (S3),²⁴ perylene (GJ-BP)²⁵ and arene derivatives (LD4),²⁶ etc. Additionally, anthracene has also been used as a good π -spacer in porphyrin and organic dyes.^{12,27-31}

In addition to converting solar energy under one-sun

irradiation for outdoor applications, DSSC has the potential to perform very efficiently under low light conditions for indoor applications. To explore this possibility, several studies have been conducted in the past few years.³²⁻³⁹ Among them, we reported a cost-effective and fairly efficient anthracene-based dye (AN-3) for DSSC under indoor conditions.³⁴ In said work, a large and flexible module (active area = 36.00 cm²) sensitized with the AN-3 dye attained a power conversion efficiency (PCE) of 5.45 % under 1000 lux of T5 fluorescent light, slightly inferior to the 5.67% PCE of the Z907 module.



Scheme 1 Chemical structures of the AN dyes.

In this work, we modified both the dyes and the solar modules to achieve a higher PCE. For the dyes, modification of the AN-3 dye yielded three new photo-sensitizers, denoted as AN-11, AN-12, and AN-14. Chemical structures of the new AN dyes are shown in Scheme 1. For AN-11, we modified the AN-3 dye³⁴ with an additional benzothiadiazole (BTDA) group which serves as a stronger electron-withdrawing motif. BTDA has been a well reported as a good acceptor in the literature.^{18,40-42}

^a Department of Applied Chemistry, National Chi Nan University, No. 302 University Road, Puli, Nantou Hsien 54561, Taiwan (R.O.C.). Fax: +886-49-2917956; Tel: +886-49-2910960 ext. 4152

^b Taiwan DSC PV Ltd., No. 3, Guojian 1st Rd., Guanyin Dist., Taoyuan City 32844, Taiwan (R.O.C.)

* To whom correspondence should be addressed - E-mail: cyl@ncnu.edu.tw
Electronic Supplementary Information (ESI) available: [Dye synthesis, characterization, and selected photovoltaic data]. See DOI: 10.1039/x0xx00000x

ARTICLE

Journal Name

The benefits of using BTDA include boosting the charge transfer processes, extending the π -conjugation, and enhancing light-harvesting ability of the dyes. With BTDA, one could expect a stronger push-pull tendency of the new AN dyes and, hopefully, a higher PCE of the devices. For AN-12 and AN-14, an *N,N*-diarylamino-anthryl group is used as the common donor, and a cyano-acrylic acid or a carboxylic acid is employed as the anchoring groups, respectively. *N,N*-diarylamino-anthryl groups are effective electron-donating groups and they have been successfully used as the donor of several efficient organic and porphyrin dyes.^{39,43,44} Cyano-acrylic acid and carboxylic acid are widely used anchoring groups with electron-withdrawing property.^{20,45-47} Based on this design, all AN dyes should have good push-pull tendency, and the comparison should provide insight into molecular design of photo-sensitizers for indoor applications.

For the devices, three types of solar cell/modules were prepared, including lab-made small cells with an active area of 0.25 cm², the R26 rigid modules with an active area of 26.80 cm², and the F17 flexible modules with an active area of 19.80 cm². The small cells were prepared in our laboratory and the modules were manufactured by Taiwan DSC PV Ltd. (or TDP). For the small cells, photovoltaic measurements were carried out under 100 mW/cm² simulated AM1.5G sunlight to imitate the out-door condition, as well as under 200, 600, and 1000 lux of T5 or LED lights to represent indoor conditions of a dim room, a common office, and a convenient store, respectively. All AN dyes were examined in the small cells and the superior dye was chosen to sensitize the modules for further tests. For the modules, only indoor conditions were tested.

As such, our study showed that an R26 module sensitized with the AN-11 dye achieved a PCE of 11.94% under 1000 lux of T5 fluorescent light, outperforming the Z907 counterpart. Fig. 1 collects the pictures of AN-11 in a THF solution, as powders, and the solar devices sensitized with AN-11.

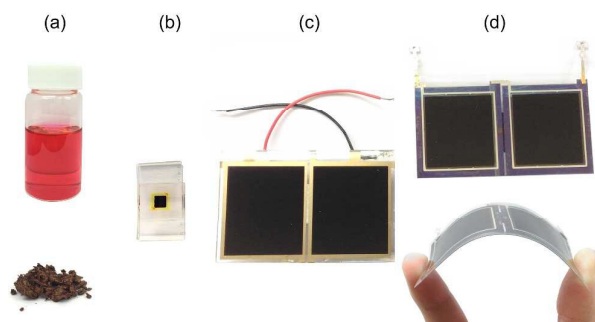


Fig. 1 Pictures of AN-11 (a) in a THF solution (top) and as powders (bottom), (b) the small cell, (c) the R26 rigid module, and (d) the F17 flexible module.

Results and discussion

Absorption and fluorescence emission spectra.

The UV-Vis absorption and fluorescent emission spectra of the AN dyes in THF are compared in Fig. 2. The related

parameters are listed in Table 1. For comparison, AN-3 is also included in Fig. 2.

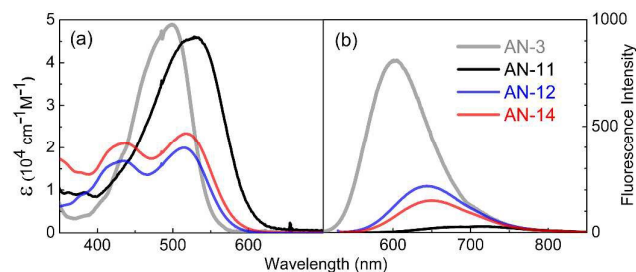


Fig. 2 (a) Absorption and (b) fluorescence emission spectra (2.0×10^{-6} M) of the AN dyes in THF.

Table 1 Spectral and electrochemical properties of the AN dyes

| Dye | Absorption, nm (ϵ , $10^4 \text{ M}^{-1} \text{ cm}^{-1}$) | Emission, ^a nm | $E_{0,0}$ V vs. SCE | | $E_{0,0}$, eV |
|-------|--|------------------------------|---------------------|------------------|-------------------|
| | | | Ox ^c | Red ^d | |
| AN-11 | 528 (4.61) | 722 | +0.85 | -1.15 | 2.08 |
| AN-12 | 433 (1.68), 515 (1.99) | 644 | +1.07 | -1.17 | 2.16 |
| AN-14 | 438 (2.10), 517 (2.34) | 652 | +1.08 | -1.09 | 2.14 |

^a 2.0×10^{-6} M of the AN dyes in THF, excitation wavelength/nm: AN-11, 528; AN-12, 515; AN-14, 517. ^b0.5 mM of the AN dyes in THF/0.1 M TBAP/N₂; Pt working and counter electrodes; SCE reference electrode; scan rate = 100 mV s⁻¹. ^cPotentials were determined by differential pulse voltammetry due to the less reversible oxidation waves. ^dPotentials were obtained by cyclic voltammetry. ^e $E_{0,0}$ values were determined by the intersection of normalized UV-visible and fluorescent spectra.

As shown in the figure, the UV-visible spectrum of AN-11 is consistent with that of the AN-3 parent with deviations. For instance, AN-3 and AN-11 both give rise to one overlapped absorption band around 500 nm with similar molar absorptivities. However, the absorption maximum of AN-11 ($\lambda_{\text{max}} = 528$ nm) is red-shifted from that of AN-3 ($\lambda_{\text{max}} = 499$ nm). This deviation may be attributed to more conjugated double bonds in the chemical structure. For AN-12 and AN-14, the spectral features are quite different from those of AN-3 and AN-11. For example, AN-12 (433 and 515 nm) and AN-14 (438 and 517 nm) exhibit two well-resolved and weaker absorption bands. This difference may be related to the different electron-donating groups and/or the electron-acceptors/anchors in the chemical structures. Among the AN dyes, absorption maxima of the lowest-energy absorption bands show a trend of AN-11 > AN-14 > AN-12 > AN-3. These absorption wavelengths are appropriate for indoor solar-cell applications.

For fluorescence, the emissions are mirror images of the corresponding lowest-energy absorptions. As expected, the emission bands are red-shifted from the corresponding absorption bands, centred at 722 nm for AN-11, 644 nm for AN-12, and 652 nm for AN-14. The trend of these wavelengths is consistent with that of the lowest-energy absorption bands, *i.e.* AN-11 > AN-14 > AN-12 > AN-3. Interestingly, the fluorescence emission of AN-11 seems very weak compared with those of AN-12 and AN-14 at the same concentration. This phenomenon may be related to molecular aggregation of

the AN-11 dye. More discussion is given in the photovoltaic section to address this possibility.

Electrochemistry, molecular orbitals and energy levels.

Fig. 3 shows the cyclic voltammograms (CV) of the AN dyes in THF. The redox potentials are listed in Table 1. Due to the less reversible nature of the oxidation reactions, differential pulse voltammograms (DPV) were also obtained to help determine the oxidation potentials.

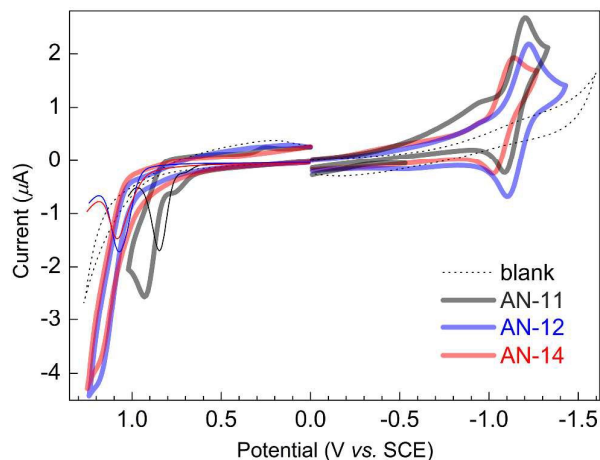


Fig. 3 Cyclic voltammograms (bold lines) of the AN dyes in THF/TBAP. For the oxidation, differential pulse voltammograms were also measured (thin lines) to help determine the potentials. Experimental conditions: [AN-x] = 0.5 mM in 0.1 M TBAP/THF, N₂, Pt working and counter electrodes, SCE.

As shown in the figure and table, the first oxidations of AN-11, AN-12 and AN-14 are found at +0.85, +1.07 and +1.08 V vs. SCE, respectively. These reactions are consistent with the formation of the cation radicals.³⁴ The first oxidation potential of AN-11 is very similar to that of AN-3 (+0.86 V vs. SCE).³⁴ This is consistent with the fact that the two dyes share a common electron-donor in the chemical structures. For AN-12 and AN-14, the first oxidation potentials are noticeably more positive than those of AN-3 and AN-11. This may be due to the different donor groups, *i.e.* *N,N*-di-octylaminophenyl-ethynyl group vs. *N,N*-di-aryl amino group.⁴⁴ Between AN-12 and AN-14, we observed similar oxidation potentials, consistent with their identical electron-donating group.

For reductions, there are ill-shaped waves near -0.80 V vs. SCE. These reactions have been established to be reduction reactions of the anchoring groups.⁴⁸ Additionally, *quasi*-reversible reactions are found at -1.15, -1.17 and -1.09 V vs. SCE for AN-11, AN-12 and AN-14, respectively. These reactions are consistent with the formation of the anion radicals.³⁴ These reduction potentials are all positively shifted from that of AN-3 (-1.43 V vs. SCE), likely due to the electron-withdrawing BTDA motif in the chemical structures. As shown in Table 1, AN-11 (-1.15 V) and AN-12 (-1.17) show similar reduction potentials possibly due to the identical electron-acceptor/anchor group. With a different acceptor/anchor, the reduction potential of AN-14 (-1.09 V) is further positive-

shifted from those of AN-11 and AN-12. This further positive shift may be attributed to the BTDA motif and the additional, electron-withdrawing cyano group in the chemical structure. These assignments are consistent with the calculated MO patterns.

To help qualitatively understand the frontier molecular orbitals (MO) of the AN dyes, density-functional theory (DFT) calculations were carried out at the B3LYP/6-31G(d,p) level of theory.⁴⁹ As shown in Fig. 4, electron densities of the highest occupied molecular orbitals (HOMO) mainly reside at the donors and the anthryl parts for all AN dyes. In contrast, electron probabilities of the lowest unoccupied molecular orbitals (LUMO) largely concentrate at the acceptor/anchoring and the anthryl units. First of all, these MO patterns agree well with the electrochemistry results, *i.e.* the oxidation reactions are related to the electron-donating part of the molecules whereas the reductions are related to electron-withdrawing section of the chemical structures. Secondly, uneven distribution of the electron densities/probabilities at the HOMO/LUMO levels translates to a push-pull tendency of the dyes. This tendency would result in pushing electron density from the donors toward the anchors upon photo-excitation of the dyes. This is a welcome merit for n-type DSSC applications. Thirdly, the electron densities/probabilities seem to be more localized for the HOMO and LUMO of AN-11 than those of AN-3, suggesting a stronger push-pull tendency of the AN-11 dye upon excitation. This suggestion is consistent with the DFT-calculated dipole moments (AN-3: 7.96 Debyes, AN-11: 8.65 Debyes). The increased dipole moment of AN-11 may be attributed to the presence of BTDA motif in the structure.

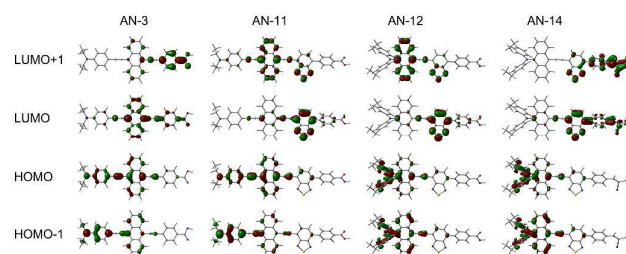


Fig. 4 Frontier molecular orbitals of AN-3, AN-11, AN-12 and AN-14. Calculation method: Gaussian 03W, DFT, B3LYP/6-31G(d,p).

Fig. 5 compares the energy levels of the HOMO/LUMO of each dye, the conduction bands (CB) of TiO₂ and the redox potential of the electrolyte (I⁻/I₃⁻).² The HOMO/LUMO levels are based on the corresponding redox potentials of each dye. As clearly shown in the figure, the LUMO levels of the AN dyes are considerably higher than the conduction bands (CB) of TiO₂ and the HOMO levels are noticeably lower than the energy level of the electrolyte. Therefore, the AN dyes should all be capable of injecting electrons into the CB of TiO₂ upon excitation, and the resulting cations should be efficiently regenerated by the electrolyte. A similar diagram comparing the ground/excited states of each dye is also provided in the ESI (Fig. S1). In short, the afore-mentioned conclusion also applies to Fig. S1.

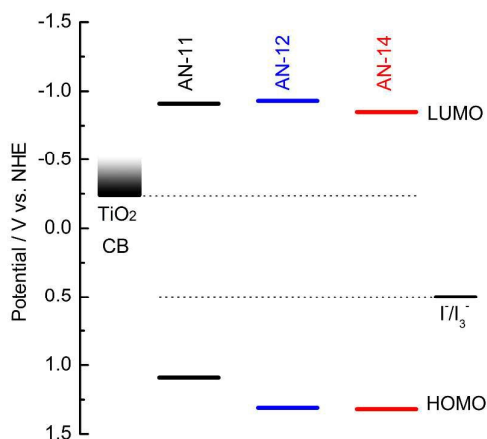


Fig. 5 Energy-level diagram of the AN dyes, the electrolyte and TiO₂.

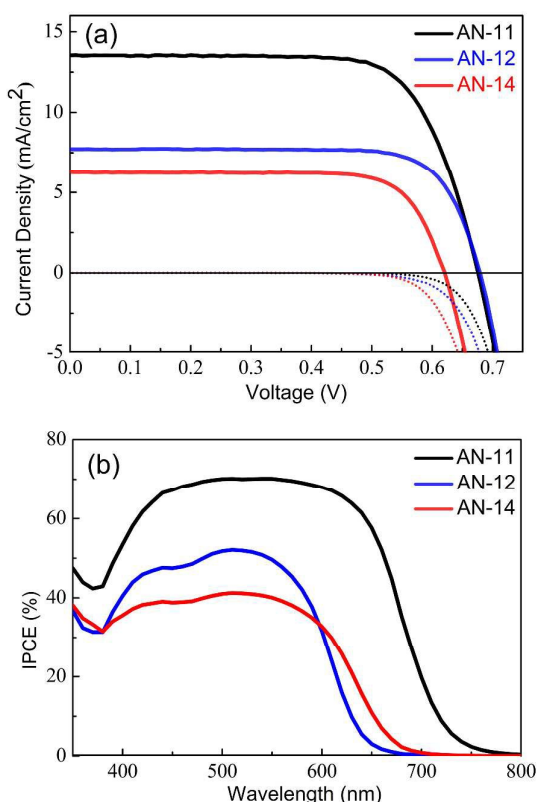


Fig. 6 (a) The J - V curves (dashed lines: dark currents) and (b) IPCE spectra under 100 mW cm^{-2} simulated AM1.5G sunlight.

Photovoltaic properties of the small cells.

The small cells are prepared in our laboratory with an active area of 0.25 cm^2 . A black mask with an aperture area of 0.16 cm^2 was applied to the small cells during the photovoltaic measurements. For the measurements, 100 mW/cm^2 simulated AM 1.5G sunlight (or one-sun) was applied to represent the outdoor environment. Fig. 6 shows the (a) current density-voltage (J - V) curves and (b) incident photon-to-current conversion efficiency (IPCE) spectra of the AN small

cells under one-sun irradiation. The related parameters are tabulated in Table 2. For comparison, data of the Z907 small cells were also included in Table 2.

Table 2 Photovoltaic Properties of the AN and Z907 small cells under simulated AM 1.5 Irradiation (100 mW/cm^2)^a

| Entry | $J_{sc}^{IPCE,b}$ (mA/cm^2) | J_{sc} (mA/cm^2) | V_{oc} (mV) | FF (%) | η (%) | Dye loading (nmol/cm^2) |
|-------|---|----------------------------------|------------------|--------------|-----------------|---------------------------------------|
| AN-11 | 12.70 | 13.09 ± 0.32 | 680 ± 1.0 | 71 ± 1.0 | 6.36 ± 0.18 | 300 |
| AN-12 | 6.60 | 7.43 ± 0.18 | 680 ± 1.0 | 76 ± 1.0 | 3.87 ± 0.11 | 290 |
| AN-14 | 6.05 | 6.27 ± 0.17 | 600 ± 1.0 | 78 ± 1.0 | 2.96 ± 0.12 | 370 |
| Z907 | 13.34 | 16.29 ± 0.37 | 763 ± 6.0 | 70 ± 1.0 | 8.69 ± 0.33 | - |

^aThe active area was 0.25 cm^2 with a black mask of area 0.16 cm^2 . The parameters are the averaged values of various number of independent devices (AN-11 = 16 cells, AN-12 = 5 cells, AN-14 = 7 cells, Z907 = 5 cells). ^b J_{sc}^{IPCE} is derived via wavelength integration of the IPCE spectra to compare with the J_{sc} values obtained from the J - V measurements.

As shown in Table 2, the overall efficiencies of the small cells exhibit a trend of AN-11 > AN-12 > AN-14 under one-sun irradiation. The AN-11 cell outperforms the AN-12 and AN-14 cells with $J_{sc} = 13.09 \text{ mA/cm}^2$, $V_{oc} = 680 \text{ mV}$, $FF = 71\%$, and a PCE of 6.36%. Upon closer inspection, we observed similar dye-loadings of the AN cells. In addition, the V_{oc} value of the AN-11 cell is similar to that of the AN-12 cell but moderately greater than that of the AN-14 cell. Therefore, these results would suggest that a greater J_{sc} value may be a more important factor contributing to the greater PCE of the AN-11 small cell. A greater J_{sc} value of the AN-11 cell is consistent with the more broadened and intensified IPCE spectrum (Fig. 6b). This suggestion is supported by the integrated values of the IPCE responses (J_{sc}^{IPCE}). As compared in Table 2, the J_{sc}^{IPCE} values show the same trend as in the J - V study, *i.e.* AN-11 > AN-12 > AN-14. As for the fill factors (FF), FF value of the AN-11 cell (71%) is noticeably lower than those of the AN-12 (76%) and AN-14 (78%) cells. Given the same cell fabrication procedure and the small deviations of the averaged values, the lower FF value of the AN-11 cell may not be caused by defects of the device. As such, the lower FF value of the AN-11 cell could be related to the nature of the dye.⁵⁰ As shown in Fig. 1, the chemical structures of AN-12 and AN-14 are similar to each other, but different from that of AN-11. As shown in Table 1, the oxidation potentials and the absorption wavelengths of AN-12 and AN-14 are similar to each other, but different from those of AN-11. These differences may have impacts to the photovoltaic parameters, such as the FF values.

The very broad IPCE spectrum of the AN-11 cell is consistent with the colour of the device (Fig. 1b-1d). With a relatively simple chemical structure, it is expected to observe an absorption band of AN-11 at 528 nm (Fig. 2a). As a result, the AN-11 solution appears red (Fig. 1a). Much to our surprise, the AN-11 solar devices show a very black colour. To better understand the differences in colour, Fig. 7 collects normalized UV-visible and IPCE spectra. Between the solution and the film spectra, the absorption bands of the film spectra (red dotted curves) are slightly shifted and broadened from those of the AN solutions (black curves). These spectral changes may be

related to intermolecular interactions of the dye molecules on the surfaces of TiO₂ nanocrystalline films. It has been well documented that the face-to-face, H-type aggregation of π -molecules generates a blue shift of the absorption band(s), whereas the tilted (or head-to-tail), J-type aggregation results in a red shift.⁵¹ Therefore, the blue-shifted film spectrum of AN-11 suggests H-type aggregation, and the red-shifted film spectra of AN-12 and AN-14 suggest J-type aggregation of the dye molecules on TiO₂. In addition, the broadening phenomenon seems to be more apparent for the AN-11 film. This implies that AN-11 may be more susceptible to aggregation than are the AN-12 and AN-14 dyes. This suggestion is consistent with the much weaker fluorescence emission of the AN-11 solution shown in Fig. 2b. Note that the afore-mentioned solutions are dilute and the films only adsorb limited amount of the dye molecules to avoid saturation of the absorption bands. As the amounts of the dyes increase, one should observe further broadening of the film spectra. To examine this possibility, Fig. 7 also includes normalized IPCE spectra of the AN small cells (blue bold curves). Note that, in this case, much more dye molecules were allowed to adsorb onto the photo-anodes (Table 2). Due to the amounts of the dyes, severe saturation was observed for the UV-visible spectra of the photo-anodes, rendering the spectra unusable. Therefore, we hope to represent the region of the absorptions of the photo-anodes by comparing the IPCE spectra. As clearly shown in Fig. 7, the IPCE spectrum of the AN-11 small cell is significantly more broadened than those of the AN-12 and AN-14 counterparts, resulting in a panchromatic IPCE spectrum covering the entire visible region from 350 to 750 nm. Consequently, the AN-11 cell exhibits a very black colour. To demonstrate the blackness of the AN-11 devices, large R26 modules sensitized with the AN-11, Z907, and AN-3 dyes are compared in Fig. 8. As shown in the figure, the AN-11 module gives rise to a very black colour whereas the Z907 and the AN-3 modules show a brown and an orange colour, respectively.

Electrochemical impedance spectroscopy (EIS) was also carried out in order to reveal important interfacial charge-transfer processes. Fig. 9 compares Nyquist plots of the AN small cells in the dark. Three semicycles are expected from 0.1 Hz to 1 MHz for each cell, including one small semicircle in the lower frequency range (from 0.1 Hz to 2 Hz), one larger semicircle in the middle frequency range (from 2 Hz to 1 kHz), and another smaller semicircle in the highest frequency range (>1 kHz). These semicycles are related to the ion diffusion in the electrolyte, the charge-transfer processes at the TiO₂/dye/electrolyte interface, and the charge-transfer processes at the Pt/electrolyte interface, respectively. As expected, the semicycles in the highest frequency range (or left side of the figure) are similar for all AN cells. For the semicycles at the lower frequency range (right side), the signals are obscured by the large semicycles at the middle frequencies. Importantly, the middle semicircle of the AN-11 cell is significantly larger/broader than those of the AN-12 and AN-14 cells. This suggests a lower charge recombination rate thus a weaker dark current for the AN-11 cells (Fig. 6a),

contributing to the superior photovoltaic performance. This is consistent with the *J-V* and IPCE measurements.

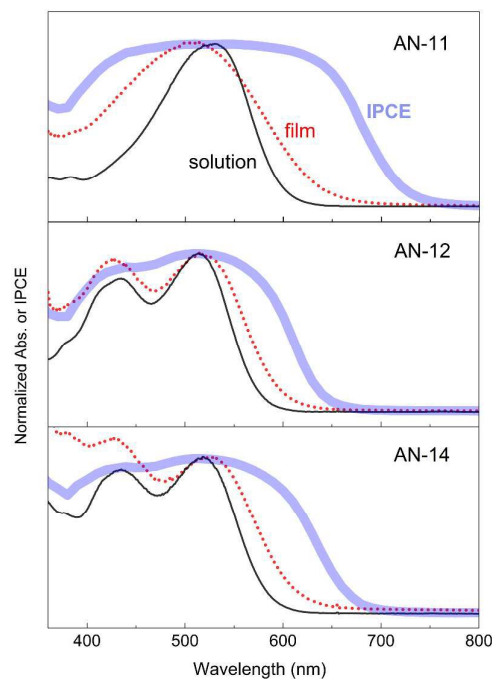


Fig. 7 Comparison of the solution UV-visible spectra (black solid) with the film spectra (red dotted), and with the IPCE spectra (bold blue) of AN-11 (top), AN-12 (middle), and AN-14 (bottom).

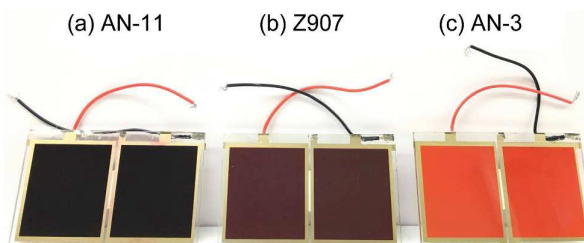


Fig. 8 R26 modules sensitized with (a) AN-11, (b) Z907, and (c) AN-3.

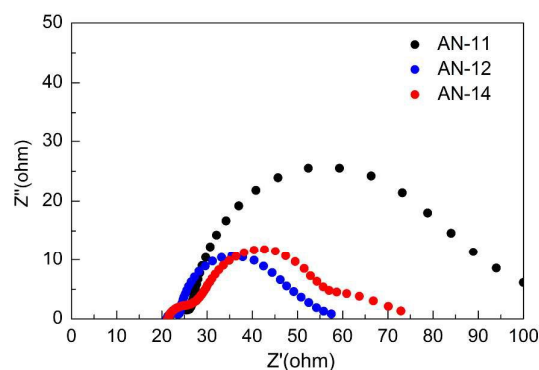


Fig. 9 EIS Nyquist plots of the AN cells in the dark.

Table 3 Photovoltaic parameters of the R26 modules under T5 and LED lights

| Light source ^a | Dye ^b | Photon flux (lux) | J_{sc} ($\mu\text{A}/\text{cm}^2$) | V_{oc} (mV) | FF (%) | P_{in} ($\mu\text{W}/\text{cm}^2$) | P_{max} ($\mu\text{W}/\text{cm}^2$) | η (%) |
|---------------------------|------------------|-------------------|--|---------------------|------------------|--|---|------------------|
| T5 | AN-11 | 200 | 10.90 \pm 0.10 | 906.20 \pm 19.40 | 64.30 \pm 1.40 | 70 | 6.38 \pm 0.08 | 9.08 \pm 0.11 |
| | | 600 | 34.40 \pm 0.30 | 1007.80 \pm 24.50 | 65.50 \pm 1.00 | 203 | 22.68 \pm 0.37 | 11.17 \pm 0.18 |
| | | 1000 | 61.50 \pm 0.60 | 1050.90 \pm 24.90 | 64.30 \pm 1.10 | 348 | 41.56 \pm 0.56 | 11.94 \pm 0.16 |
| | Z907 | 200 | 10.00 \pm 0.10 | 941.30 \pm 5.40 | 64.80 \pm 0.60 | 70 | 6.11 \pm 0.03 | 8.69 \pm 0.04 |
| | | 600 | 31.60 \pm 0.30 | 1058.00 \pm 5.70 | 64.90 \pm 0.60 | 203 | 21.73 \pm 0.17 | 10.70 \pm 0.08 |
| | | 1000 | 56.60 \pm 0.60 | 1104.40 \pm 5.60 | 64.10 \pm 0.80 | 348 | 40.03 \pm 0.00 | 11.50 \pm 0.11 |
| LED | AN-11 | 200 | 10.40 \pm 0.10 | 908.20 \pm 19.90 | 64.50 \pm 1.50 | 63 | 6.10 \pm 0.08 | 9.68 \pm 0.13 |
| | | 600 | 31.60 \pm 0.30 | 999.20 \pm 21.60 | 65.60 \pm 1.20 | 189 | 20.72 \pm 0.33 | 10.95 \pm 0.17 |
| | | 1000 | 52.90 \pm 0.60 | 1038.70 \pm 24.30 | 64.70 \pm 1.20 | 316 | 35.58 \pm 0.67 | 11.26 \pm 0.21 |
| | Z907 | 200 | 9.60 \pm 0.10 | 942.80 \pm 6.50 | 64.80 \pm 0.70 | 63 | 5.86 \pm 0.06 | 9.30 \pm 0.09 |
| | | 600 | 29.40 \pm 0.20 | 1052.80 \pm 6.20 | 65.10 \pm 0.60 | 189 | 20.14 \pm 0.18 | 10.64 \pm 0.10 |
| | | 1000 | 48.80 \pm 0.50 | 1093.50 \pm 5.70 | 64.60 \pm 0.70 | 316 | 34.46 \pm 0.34 | 10.91 \pm 0.11 |

^a T5 fluorescent light and LED were manufactured by China Electric MFG. Co. ^bNumber of the modules: 5.

As for the indoor performance of the AN small cells, photovoltaic data of the small cells under 1000 lux of T5 or LED lights were tabulated in the ESI (Table S1). In short, the same trend is observed, *i.e.* AN-11 > AN-12 > AN-14. Therefore, AN-11 is chosen to sensitize the modules for the following investigation.

Photovoltaic and stability tests of the modules.

For practical applications, photovoltaic measurements of large modules were also evaluated. As mentioned above, AN-11 was used to sensitize the modules because it outperformed other AN dyes in the small-cell tests. Two types of modules were manufactured by Taiwan DSC PV Ltd. for the following tests. The R26 module is rigid with an active area of 26.80 cm² and the F17 module is flexible with an active area of 19.80 cm² (Fig. 1). No masks were applied during the measurements and only indoor conditions were tested due to the architectural limitations of the modules. For the light sources, 200 - 1000 lux of T5 or LED lights were used to represent various indoor illumination conditions, ranging from a dim room, a common office, to that of a convenient store.

Table 3 summarizes the photovoltaic data of the R26 modules sensitized with AN-11 and Z907 under 200, 600, and 1000 lux of T5 and LED lights. For the Z907/R26 modules, the PCE values under 200 lux T5 and LED lights are comparable with that of the Z907 small cell under one sun irradiation. With the illuminances increased from 200 to 1000 lux, PCE of the Z907/R26 module also increased from 8.69% to 11.50% for T5 light and from 9.30% to 10.91% for LED light. For the AN-11/R26 module, the PCE values under indoor conditions are superior to that under one sun irradiation. This is consistent with the literature reports.^{10,34,35} Significantly, the AN-11/R26 module outperforms the Z907/R26 module with a PCE of 11.94% under 1000 lux of T5 light. One may consider this PCE value as highly efficient considering the large size of the R26 module. For LED light, PCE values of the AN-11/R26 modules are also greater than those of the Z907/R26 module. As for the F17 modules, the photovoltaic data are collected in Table 4. As

shown in the table, a relatively similar trend as for the rigid modules is also observed for the flexible modules. However, the F17 modules seem slightly less efficient than the R26 counterparts. Note that active areas of the modules were used to calculate the PCE values in Table 3 and 4. In addition to active area, aperture area and total area are also important factors when evaluating PCE of the modules.⁵² Therefore, we compare PCE variation of the modules based on different area dimensions in Table S2 and S3, ESI.

Differences in the photovoltaic properties of the modules may be related to the differences in the emission spectra of the artificial light sources. Fig. 10 compares the UV-Vis absorption spectra of AN-11 and Z907 with the emission spectra of the T5 and LED lights. As shown in the figure, the absorption ranges of the two dyes are suitable for indoor photovoltaic applications. Between the two dyes, AN-11 exhibits a much greater extinction coefficient and a wider light-absorption range, possibly contributing to the superior performance of the AN-11 modules under indoor irradiation.

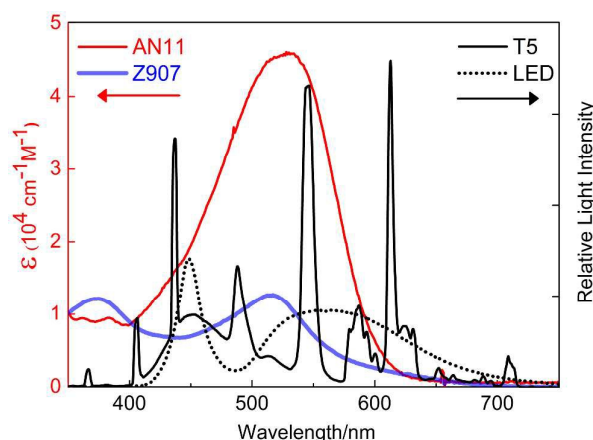


Fig. 10 Absorption spectra of AN-11 and Z907 vs. the T5 and LED emission spectrum.

Table 4 Photovoltaic parameters of the F17 modules under T5 and LED lights

| Light source ^a | Dye ^b | Photon flux (lux) | J_{sc} ($\mu\text{A}/\text{cm}^2$) | V_{oc} (mV) | FF (%) | P_{in} ($\mu\text{W}/\text{cm}^2$) | P_{max} ($\mu\text{W}/\text{cm}^2$) | η (%) |
|---------------------------|------------------|-------------------|--|--------------------|------------------|--|---|-----------------|
| T5 | AN-11 | 200 | 7.70 \pm 0.20 | 929.40 \pm 4.10 | 76.00 \pm 0.90 | 67 | 5.46 \pm 0.10 | 8.15 \pm 0.15 |
| | | 600 | 24.40 \pm 0.80 | 1008.40 \pm 4.00 | 76.30 \pm 0.80 | 203 | 18.80 \pm 0.39 | 9.26 \pm 0.19 |
| | | 1000 | 41.20 \pm 1.20 | 1039.60 \pm 2.60 | 75.80 \pm 1.30 | 338 | 32.46 \pm 0.54 | 9.60 \pm 0.16 |
| | Z907 | 200 | 7.40 \pm 0.10 | 1009.30 \pm 6.70 | 71.10 \pm 1.90 | 67 | 5.31 \pm 0.13 | 7.92 \pm 0.19 |
| | | 600 | 23.00 \pm 0.60 | 1101.00 \pm 6.40 | 73.40 \pm 1.80 | 203 | 18.53 \pm 0.18 | 9.13 \pm 0.09 |
| | | 1000 | 38.40 \pm 1.60 | 1135.30 \pm 8.60 | 75.00 \pm 1.60 | 338 | 32.70 \pm 1.27 | 9.67 \pm 0.38 |
| LED | AN-11 | 200 | 7.30 \pm 0.30 | 928.30 \pm 5.60 | 75.10 \pm 1.40 | 63 | 5.09 \pm 0.12 | 8.08 \pm 0.18 |
| | | 600 | 23.00 \pm 0.60 | 1007.90 \pm 3.70 | 75.70 \pm 0.70 | 187 | 17.52 \pm 0.35 | 9.37 \pm 0.19 |
| | | 1000 | 38.10 \pm 1.40 | 1036.90 \pm 4.40 | 76.10 \pm 1.20 | 316 | 30.07 \pm 0.79 | 9.51 \pm 0.25 |
| | Z907 | 200 | 7.00 \pm 0.20 | 1007.00 \pm 7.70 | 71.60 \pm 1.70 | 63 | 5.03 \pm 0.04 | 7.99 \pm 0.07 |
| | | 600 | 21.90 \pm 0.60 | 1101.70 \pm 8.10 | 73.40 \pm 2.00 | 187 | 17.67 \pm 0.38 | 9.45 \pm 0.20 |
| | | 1000 | 36.90 \pm 1.10 | 1138.50 \pm 6.00 | 75.20 \pm 1.40 | 316 | 31.54 \pm 0.35 | 9.98 \pm 0.11 |

^a T5 fluorescent light and LED were manufactured by China Electric MFG. Co. ^bNumber of the modules: 5.

To evaluate the stability of the modules under indoor environments, weather-stress tests were performed. The tests were carried out by TDP according to the SEMI (the global industry association serving the manufacturing supply chain for the micro- and nano-electronics industries) standards. For the rigid R26 modules, the thermal cycle test was given. In this test, surrounding temperature of the AN-11/R26 modules was cycling between 60°C and -10°C at 1°C/min rate. Photovoltaic measurements of the modules under 200 lux of T5 light showed that 90.1% of the maximal out-put power of the R26 modules remained after 50 cycles of the thermal cycle test (Fig. 11a). For the flexible F17 modules, the damp-heat test was given. In this test, the flexible modules were put under 65°C and 65% of humidity. The results showed that 87.3% of the maximal out-put power of the AN-11/F17 modules remained after 600 hours (Fig. 11b).

Finally, we conducted the studies of scaling-up, costing-down and the relationship with the photovoltaic performance. So far, our study showed that the synthesis of AN-11 can be scaled up to three grams for each reaction and the cost can be cut down to about US\$60/g. *J-V* measurements of the cost-down AN-11 small cells show no decrease in the photovoltaic performance.

Conclusion

In this work, we report the synthesis, fundamental and photovoltaic properties of three new anthracene-based organic dyes, denoted as AN-11, AN-12 and AN-14. Among the AN dyes, AN-11 shows superior photovoltaic performance than other AN dyes. Significantly, the AN-11/R26 module outperforms the Z907 counterpart with a PCE of 11.94% under 1000 lux of T5 fluorescent light. Furthermore, our study shows that photovoltaic performance of AN-11 is not affected upon scaling up the synthesis and cutting down the cost. These are the merits for industrializing AN-11 for practical applications.

Experimental

Instruments

NMR (Bruker Avance II 300 MHz), UV-visible (Agilent 8453), fluorescence (Varian Cary Eclipse), and Mass (Microfilex MALDI-TOF MS, Bruker Daltonics) spectra were obtained on the indicated instruments. Elemental analyses were carried out by the MOST Instrumentation Center at National Taiwan University (Elementar Vario EL III). Electrochemistry was carried out using a standard three-electrode cell (a Pt working electrode, a Pt auxiliary electrode, and an SCE reference electrode) on a CH Instruments Electrochemical Workstation 611A. A glove box (MBraun Uni-Lab), a vacuum line and standard Schlenk glassware were employed to process all materials sensitive to air. The current-voltage (*J-V*) characteristics of the DSSC devices covered with a black mask (aperture area $0.4 \times 0.4 \text{ cm}^2$) were determined with a solar simulator (AM 1.5G, SS50 AAAEM, PET) and a source meter

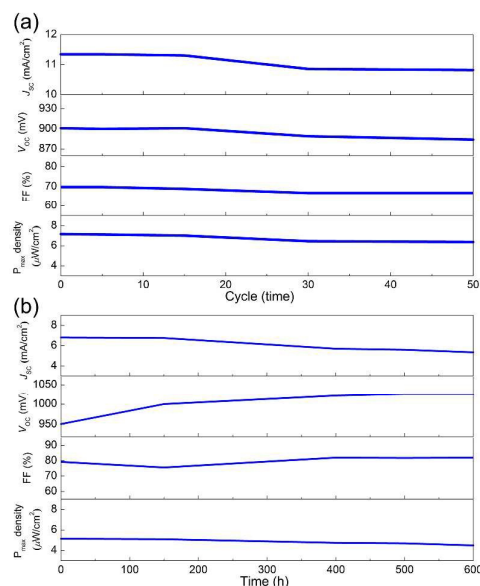


Fig. 11 Photovoltaic parameters of the (a) AN-11/R26 module and (b) AN-11/F17 module under the weather stress tests. Conditions: 200 lux of T5 light, (a) the thermal cycle test: cycling between 60°C and -10°C at 1°C/min rate.; (b) The damp-heat test: 65°C, and 65% of humidity.

ARTICLE

Journal Name

(Keithley 2400). The measurement of the incident photon-to-current conversion efficiency (IPCE) was performed by the 7-SCSpec system (Sofn Instruments Co., Ltd.) with a source meter (Keithley 2000). The dim-light conversion efficiency measurement system was purchased from Yu-Yi Enterprise Co., Ltd., Taiwan, with a spectrophotometer (Ocean Optics USB2000+UV-vis) and a source meter (Keithley 2401). The T5 and LED lights were manufactured by China Electric MFG. Co.

Materials

Solvents for the synthesis (ACS grade) were CH_2Cl_2 and CHCl_3 (Mallinckrodt Baker), hexanes (Haltermann, Hamburg, Germany), and tetrahydrofuran (THF) (Merck, Darmstadt, Germany). These solvents were used as received unless otherwise stated. Other chemicals were obtained commercially (Acros Organics). THF for cross-coupling reactions was purified and dried with a solvent-purification system (Asiawong SD-500, Taipei, Taiwan); about 50 ppm of H_2O was found in the resulting fluid. The $\text{Pd}(\text{PPh}_3)_4$ catalyst (Strem, MA, USA) was used as received. For electrochemical measurements, THF was distilled over sodium under N_2 . For chromatographic purification, we used silica gel 60 (230–400 mesh, Merck).

Device fabrication

R26 and F17 modules were fabricated by Taiwan DSC PV Ltd. (<http://www.tdp-dsc.com>). For the small cells, a screen-printed, bi-layer TiO_2 film on a pre-cleaned and TiCl_4 -treated fluorine doped tin oxide (FTO) conducting glass (TEC 7, Hartford, U.S.A.) was prepared as the working electrode. A screen-printed Pt on an FTO glass was used as the counter electrode. The TiO_2 bi-layer film of the working electrode consists of a 9- μm translucent layer of small particles (15–20 nm, Ti-2105A, Eternal Materials Co., Ltd.) and a 6- μm light-scattering layer of large TiO_2 particles (~ 300 nm, Ti-2325, Eternal Materials Co., Ltd.). The active size of the TiO_2 film was $0.5 \times 0.5 \text{ cm}^2$. The post sintering procedures of the working and the counter electrodes are as those in our previous work.³⁴ Dye-soaking procedure of the working electrode involves immersing the photo-anodes in a toluene/ethanol ($v/v = 1/1$) solution containing 0.20 mM of the dye for 5 hours. The working and the counter electrodes were hot-pressed into one sandwich cell with a 25- μm surllyn film. The electrolyte injected into the sandwich cell contained I_2 (0.05 M), LiI (0.125 M), 3-propyl imidazolium iodide (PMII) (1.0 M), and 4-*t*-butylpyridine (0.75 M) in a acetonitrile/valeronitrile solvent ($v/v = 85/15$). Finally, the injection holes were sealed with another layer of surllyn films (100 μm) and a microslide glass. A mask with an aperture area of 0.16 cm^2 was applied to the small cell during the photovoltaic measurements. Dye loadings of the working electrodes were estimated by treating the working electrode with a THF solution containing 0.1 M tetrabutylammonium hydroxide (TBAOH) to desorb the dye molecules from the TiO_2 surfaces. The Z907 small cells were fabricated according to the same procedure except for the dye-soaking condition and the composition of the electrolyte.⁹

Dye synthesis

Syntheses of the AN dyes are based on the Sonogashira cross-coupling method,^{53,54} and are similar to those in our previous reports.^{34,44} Detailed procedures and characterization data are provided in the ESI.

Acknowledgements

We are grateful for the financial support from the Ministry of Science and Technology of Taiwan (MOST 105-2119-M-260-001 and MOST-103-2119-M-260-002).

References

- 1 B. O'Regan and M. Grätzel, *Nature*, 1991, **353**, 737-740.
- 2 M. Grätzel, *Nature*, 2001, **414**, 338-344.
- 3 S. Chakraborty, H.-C. You, C.-K. Huang, B.-Z. Lin, C.-L. Wang, M.-C. Tsai, C.-L. Liu and C.-Y. Lin, *J. Phys. Chem. C*, 2017, **121**, 7081-7087.
- 4 J. Kong, M. Mohadjer Beromi, M. Mariano, T. Goh, F. Antonio, N. Hazari and A. D. Taylor, *Nano Energy*, 2017, **38**, 36-42.
- 5 M. K. Nazeeruddin, F. De Angelis, S. Fantacci, A. Selloni, G. Viscardi, P. Liska, S. Ito, B. Takeru and M. Gratzel, *J. Am. Chem. Soc.*, 2005, **127**, 16835-16847.
- 6 M. Gratzel, *Inorg. Chem.*, 2005, **44**, 6841-6851.
- 7 F. Gao, Y. Wang, D. Shi, J. Zhang, M. Wang, X. Jing, R. Humphry-Baker, P. Wang, S. M. Zakeeruddin and M. Gratzel, *J. Am. Chem. Soc.*, 2008, **130**, 10720-10728.
- 8 C. Y. Chen, M. Wang, J. Y. Li, N. Pootrakulchote, L. Alibabaei, C. H. Ngoc-le, J. D. Decoppet, J. H. Tsai, C. Gratzel, C. G. Wu, S. M. Zakeeruddin and M. Gratzel, *ACS Nano*, 2009, **3**, 3103-3109.
- 9 Y. Cao, Y. Bai, Q. Yu, Y. Cheng, S. Liu, D. Shi, F. Gao and P. Wang, *J. Phys. Chem. C*, 2009, **113**, 6290-6297.
- 10 A. Yella, H. W. Lee, H. N. Tsao, C. Yi, A. K. Chandiran, M. K. Nazeeruddin, E. W. Diau, C. Y. Yeh, S. M. Zakeeruddin and M. Gratzel, *Science*, 2011, **334**, 629-634.
- 11 J. Luo, M. Xu, R. Li, K. W. Huang, C. Jiang, Q. Qi, W. Zeng, J. Zhang, C. Chi, P. Wang and J. Wu, *J. Am. Chem. Soc.*, 2014, **136**, 265-272.
- 12 C.-L. Wang, J.-Y. Hu, C.-H. Wu, H.-H. Kuo, Y.-C. Chang, Z.-J. Lan, H.-P. Wu, E. Wei-Guang Diau and C.-Y. Lin, *Energy Environ. Sci.*, 2014, **7**, 1392.
- 13 L. Cabau, C. Vijay Kumar, A. Moncho, J. N. Clifford, N. López and E. Palomares, *Energy Environ. Sci.*, 2015, **8**, 1368-1375.
- 14 Y. Xie, Y. Tang, W. Wu, Y. Wang, J. Liu, X. Li, H. Tian and W. H. Zhu, *J. Am. Chem. Soc.*, 2015, **137**, 14055-14058.
- 15 T. Higashino, K. Kawamoto, K. Sugiura, Y. Fujimori, Y. Tsuji, K. Kurotobi, S. Ito and H. Imahori, *ACS Appl Mater Interfaces*, 2016, **8**, 15379-15390.
- 16 S. Mathew, A. Yella, P. Gao, R. Humphry-Baker, B. F. Curchod, N. Ashari-Astani, I. Tavernelli, U. Rothlisberger, M. K. Nazeeruddin and M. Gratzel, *Nat. Chem.*, 2014, **6**, 242-247.
- 17 K. Kakiage, Y. Aoyama, T. Yano, K. Oya, J. Fujisawa and M. Hanaya, *Chem. Commun.*, 2015, **51**, 15894-15897.
- 18 Z. Yao, H. Wu, Y. Li, J. Wang, J. Zhang, M. Zhang, Y. Guo and P. Wang, *Energy Environ. Sci.*, 2015, **8**, 3192-3197.
- 19 A. K. Biswas, A. Das and B. Ganguly, *New J. Chem.*, 2016, **40**, 9304-9312.
- 20 A. Mishra, M. K. Fischer and P. Bauerle, *Angew. Chem. Int. Ed. Engl.*, 2009, **48**, 2474-2499.
- 21 H. Imahori, T. Umeyama and S. Ito, *Acc. Chem. Res.*, 2009, **42**, 1809-1818.

- 22 G. Zhang, H. Bala, Y. Cheng, D. Shi, X. Lv, Q. Yu and P. Wang, *Chem. Commun.*, 2009, DOI: 10.1039/b822325d, 2198-2200.
- 23 H. Choi, C. Baik, S. O. Kang, J. Ko, M. S. Kang, M. K. Nazeeruddin and M. Gratzel, *Angew. Chem. Int. Ed. Engl.*, 2008, **47**, 327-330.
- 24 W. Li, Y. Wu, X. Li, Y. Xie and W. Zhu, *Energy Environ. Sci.*, 2011, **4**, 1830.
- 25 H. H. Chou, Y. C. Liu, G. Fang, Q. K. Cao, T. C. Wei and C. Y. Yeh, *ACS Appl Mater Interfaces*, 2017, DOI: 10.1021/acsami.7b11784.
- 26 C.-L. Wang, Y.-C. Chang, C.-M. Lan, C.-F. Lo, E. W.-G. Diao and C.-Y. Lin, *Energy Environ. Sci.*, 2011, **4**, 1788-1795.
- 27 K. Srinivas, K. Yesudas, K. Bhanuprakash and L. Giribabu, *J. Phys. Chem. C*, 2009, **113**, 20117-20126.
- 28 C. Teng, X. Yang, C. Yang, S. Li, M. Cheng, A. Hagfeldt and L. Sun, *J. Phys. Chem. C*, 2010, **114**, 9101-9110.
- 29 K. R. Justin Thomas, P. Singh, A. Baheti, Y.-C. Hsu, K.-C. Ho and J. T. s. Lin, *Dyes Pigment.*, 2011, **91**, 33-43.
- 30 R. Yeh-Yung Lin, H.-W. Lin, Y.-S. Yen, C.-H. Chang, H.-H. Chou, P.-W. Chen, C.-Y. Hsu, Y.-C. Chen, J. T. Lin and K.-C. Ho, *Energy Environ. Sci.*, 2013, **6**, 2477.
- 31 C.-L. Wang, J.-W. Shiu, Y.-N. Hsiao, P.-S. Chao, E. Wei-Guang Diao and C.-Y. Lin, *J. Phys. Chem. C*, 2014, **118**, 27801-27807.
- 32 F. De Rossi, T. Pontecorvo and T. M. Brown, *Applied Energy*, 2015, **156**, 413-422.
- 33 C.-P. Lee, C.-A. Lin, T.-C. Wei, M.-L. Tsai, Y. Meng, C.-T. Li, K.-C. Ho, C.-I. Wu, S.-P. Lau and J.-H. He, *Nano Energy*, 2015, **18**, 109-117.
- 34 C.-L. Wang, P.-T. Lin, Y.-F. Wang, C.-W. Chang, B.-Z. Lin, H.-H. Kuo, C.-W. Hsu, S.-H. Tu and C.-Y. Lin, *J. Phys. Chem. C*, 2015, **119**, 24282-24289.
- 35 Y.-C. Liu, H.-H. Chou, F.-Y. Ho, H.-J. Wei, T.-C. Wei and C.-Y. Yeh, *J. Mater. Chem. A*, 2016, **4**, 11878-11887.
- 36 M.-N. Lu, J.-Y. Lin and T.-C. Wei, *J. Power Sources*, 2016, **332**, 281-289.
- 37 N. Sridhar and D. Freeman, In: *26th European photovoltaic solar energy conference and exhibition*, 2011, 232-236.
- 38 M. Freitag, J. Teuscher, Y. Saygili, X. Zhang, F. Giordano, P. Liska, J. Hua, S. M. Zakeeruddin, J.-E. Moser, M. Grätzel and A. Hagfeldt, *Nat. Photonics*, 2017, **11**, 372-378.
- 39 Y. S. Tingare, N. S. n. Vinh, H.-H. Chou, Y.-C. Liu, Y.-S. Long, T.-C. Wu, T.-C. Wei and C.-Y. Yeh, *Adv. Energy Mater.*, 2017, **7**, 1700032.
- 40 Z. Y. Yao, M. Zhang, R. Z. Li, L. Yang, Y. N. Qiao and P. Wang, *Angew. Chem. Int. Ed.*, 2015, **54**, 5994-5998.
- 41 A. Yella, C. L. Mai, S. M. Zakeeruddin, S. N. Chang, C. H. Hsieh, C. Y. Yeh and M. Gratzel, *Angew. Chem. Int. Ed. Engl.*, 2014, **53**, 2973-2977.
- 42 G. Yang, Y. Tang, X. Li, H. Agren and Y. Xie, *ACS Appl Mater Interfaces*, 2017, **9**, 36875-36885.
- 43 Y. Wang, B. Chen, W. Wu, X. Li, W. Zhu, H. Tian and Y. Xie, *Angew. Chem. Int. Ed. Engl.*, 2014, **53**, 10779-10783.
- 44 C.-L. Wang, M. Zhang, Y.-H. Hsiao, C.-K. Tseng, C.-L. Liu, M. Xu, P. Wang and C.-Y. Lin, *Energy Environ. Sci.*, 2016, **9**, 200-206.
- 45 L. L. Li and E. W. Diao, *Chem. Soc. Rev.*, 2013, **42**, 291-304.
- 46 G. C. Vougioukalakis, A. I. Philippopoulos, T. Stergiopoulos and P. Falaras, *Coord. Chem. Rev.*, 2011, **255**, 2602-2621.
- 47 T. Wei, X. Sun, X. Li, H. Agren and Y. Xie, *ACS Appl Mater Interfaces*, 2015, **7**, 21956-21965.
- 48 P.-S. Chao, M.-Y. Kuo, C.-F. Lo, M.-H. Hsieh, Y.-H. Cheng, C.-L. Wang, H.-Y. Lu, H.-H. Kuo, Y.-N. Hsiao, C.-M. Wang and C.-Y. Lin, *J. Porphyr. Phthalocyanines*, 2013, **17**, 92-98.
- 49 M. J. Frisch, *Gaussian 03*, Revision D.01, Gaussian, Inc., Pittsburgh PA, 2003.
- 50 G. Kron, U. Rau and J. H. Werner, *J. Phys. Chem. B*, 2003, **107**, 13258-13261.
- 51 M. Kasha, *Radiation Research*, 1963, **20**, 55.
- 52 A. Fakharuddin, R. Jose, T. M. Brown, F. Fabregat-Santiago and J. Bisquert, *Energy Environ. Sci.*, 2014, **7**, 3952-3981.
- 53 K. Sonogashira, Y. Tohda and N. Hagihara, *Tetrahedron Lett.*, 1975, **16**, 4467-4470.
- 54 S. Takahashi, Y. Kuroyama, K. Sonogashira and N. Hagihara, *Synthesis*, 1980, **1980**, 627-630.

Graphical abstract

A large, ultra black, efficient and cost-effective dye-sensitized solar module reaches an overall efficiency of ~12 % under 1000 lux of T5 fluorescent light.

